AD-A147 405 SELF-GENERATED MAGNETIC FIELDS AND THERMAL FLUX INHIBITION(U) NAVAL RESEARCH LAB WASHINGTON DC M H EMERY ET AL. 28 SEP 84 NRL-MR-5440 1/1

UNCLASSIFIED F/G 20/5 NL

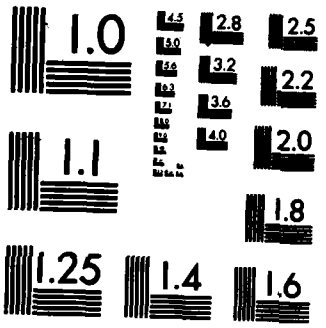
1.0
1.1
1.25
1.4
1.6
1.8
2.0
2.2
2.5
2.8
3.2
3.6
4.0
4.5
5.0
5.6
6.3
7.1

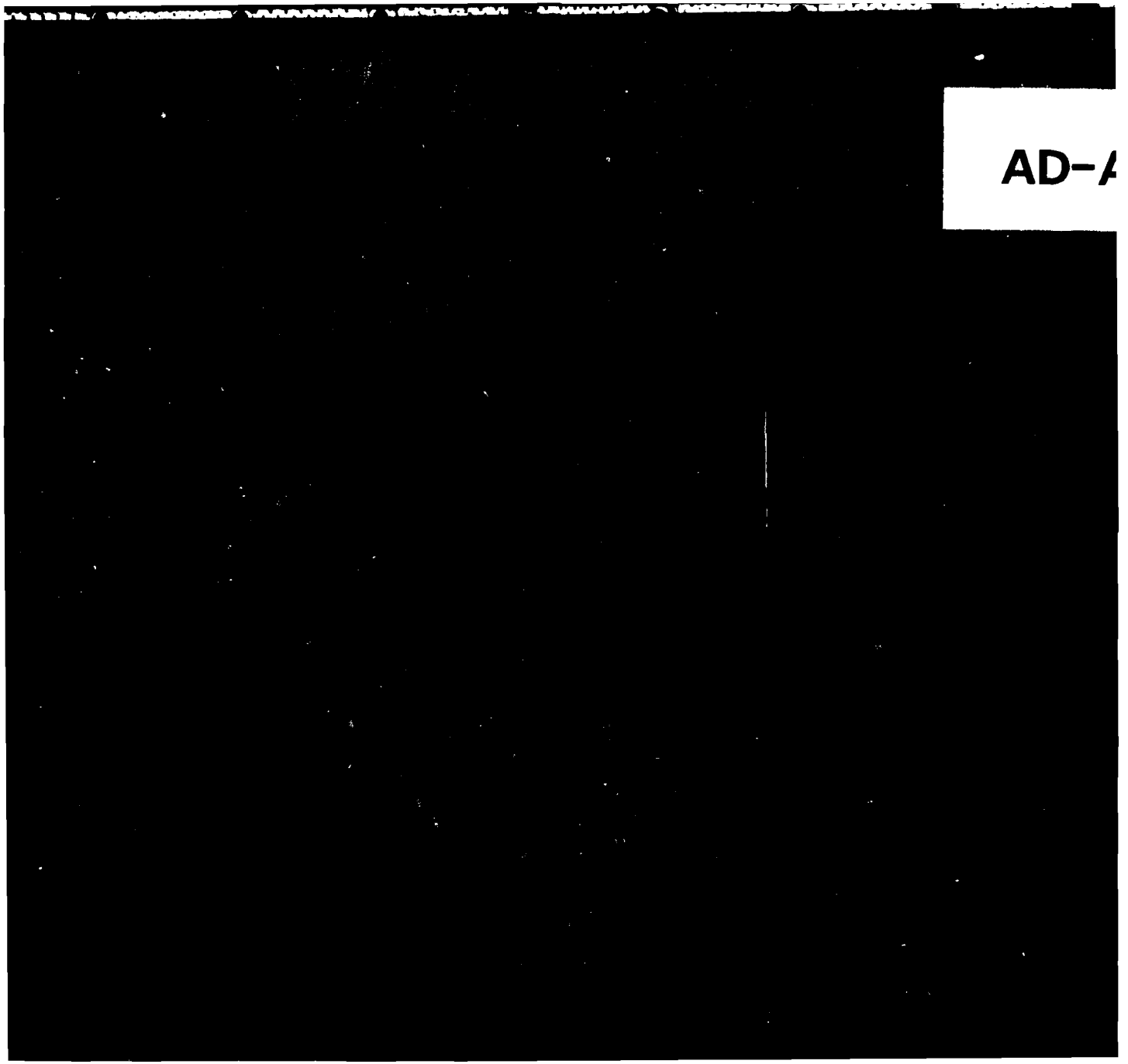
AD-A

SECURITY CLASSIFICATION OF THIS PAGE

REPORT DOCUMENTATION PAGE

1a REPORT SECURITY CLASSIFICATION UNCLASSIFIED	1b RESTRICTIVE MARKINGS
2a SECURITY CLASSIFICATION AUTHORITY	3 DISTRIBUTION / AVAILABILITY OF REPORT Approved for public release; distribution unlimited.
2b DECLASSIFICATION / DOWNGRADING SCHEDULE	
4 PERFORMING ORGANIZATION REPORT NUMBER(S) NRL Memorandum Report 5440	5 MONITORING ORGANIZATION REPORT NUMBER(S)
6a NAME OF PERFORMING ORGANIZATION Naval Research Laboratory 6b OFFICE SYMBOL (If applicable) Code 4040	7a NAME OF MONITORING ORGANIZATION
6c ADDRESS (City, State, and ZIP Code) Washington, DC 20375	7b ADDRESS (City, State, and ZIP Code)
8a NAME OF FUNDING / SPONSORING ORGANIZATION 8b OFFICE SYMBOL (If applicable)	9 PROCUREMENT INSTRUMENT IDENTIFICATION NUMBER
8c ADDRESS (City, State, and ZIP Code)	10 SOURCE OF FUNDING NUMBERS PROGRAM ELEMENT NO. / PROJECT NO. / TASK NO. / WORK UNIT ACCESSION NO. DN220-133

11 TITLE (Include Security Classification)
Self-Generated Magnetic Fields and Thermal Flux Inhibition

12 PERSONAL AUTHOR(S)
Emery, M.H. and Gardner, J.H.

13a TYPE OF REPORT	13b TIME COVERED	14 DATE OF REPORT (Year, Month, Day)	15 PAGE COUNT
Interim	FROM _____ TO _____	1984 September 28	16

16 SUPPLEMENTARY NOTATION
This work was supported by the U.S. Department of Energy and the Office of Naval Research.

17 COSATI CODES			18 SUBJECT TERMS (Continue on reverse if necessary and identify by block number)
FIELD	GROUP	SUB-GROUP	Laser-matter interaction; Thermal flux inhibition; Thermal transport; Magnetic fields (Continues)

19 ABSTRACT (Continue on reverse if necessary and identify by block number)

We show that the observed thermal flux inhibition in high intensity, short pulse laser-plasma interaction experiments can stem directly from the strong magnetic fields generated at the ablation layer as a result of laser asymmetries. The self-consistent modeling of magnetized thermal transport in this environment shows strong thermal flux inhibition as manifested by reduced ablation pressures, reduced implosion velocities, reduced classical absorption, density profile flattening and reduced mass ablation rates.

20 DISTRIBUTION / AVAILABILITY OF ABSTRACT ☒ UNCLASSIFIED/UNLIMITED ☐ SAME AS RPT ☐ DTIC USERS	21 ABSTRACT SECURITY CLASSIFICATION UNCLASSIFIED
22a NAME OF RESPONSIBLE INDIVIDUAL M. H. Emery	22b TELEPHONE (Include Area Code) (202) 767-3196 22c OFFICE SYMBOL Code 4040

DD FORM 1473, 84 MAR 83 APR edition may be used until exhausted.
All other editions are obsolete

SECURITY CLASSIFICATION OF THIS PAGE

18. SUBJECT TERMS (Continued)

Laser asymmetries
Hydrodynamics
Numerical simulation

DTIC
ELECTE
S NOV 1 4 1984 D
B

Accession For
NTIS GRA&I ☑
DTIC TAB ☐
Unannounced ☐
Justification
By
Distribution/
Availability Codes
Dist | Avail and/or Special
A-1

SELF-GENERATED MAGNETIC FIELDS AND THERMAL FLUX INHIBITION

Of critical concern in directly driven laser fusion systems is the understanding of electron thermal transport between the region where the laser light is absorbed and the ablation layer. Evidence has accumulated over the past several years which indicates that the heat flow rate may be strongly inhibited. The signatures for strongly inhibited thermal flux are increased burn-through times[1], reduced implosion velocities[2], reduced mass ablation rates[3], density profile flattening[4], significant energy losses to fast ions[5], and reduced classical absorption[6].

Computer hydrodynamics models used to interpret these experiments have typically employed strong flux-limited diffusion. These codes usually model the heat flux as $q^{-1} = q_K^{-1} + (fq_{fs})^{-1}$, where $q_K = -KT^{5/2}\nabla T$ is the classical thermal flux and K is the unmagnetized transport coefficient[7]. $q_{fs} = n_e m_e^{-1/2}(kT_e)^{3/2}$ is the free-streaming flux where n_e, m_e, T_e are the electron number density, mass and temperature, respectively. f is the flux inhibition factor. Computer modeling of both planar and spherical experiments with short pulses ($\lesssim$ 1ns), high absorbed intensities ($\gtrsim 10^{14}$ W/cm^2) at 1.054 μm laser light has led to fairly widespread acceptance of a flux inhibition value near f = 0.03. This approach is deficient in several respects not the least of which are that it is ad hoc and it avoids addressing the cause of the flux inhibition.

Several mechanisms have been proposed as being responsible for the poor transport. These include ion-acoustic turbulence[8], the Weibel instability[9], large-scale magnetic fields due to finite-sized laser spots[10], small-scale turbulent magnetic fields[11] and deficiencies in the modeling of classical diffusion[12]. Serious theoretical questions remain concerning the ability of

Manuscript approved July 11, 1984.

the first two mechanisms to provide enough inhibition and it is unlikely that magnetic fields generated solely in the underdense region or at the edge of the laser spot would be effective in inhibiting the transport. As yet, none of these mechanisms have been fully implemented into multi-dimensional hydrodynamics models to investigate the resulting flux inhibition in a self-consistent manner.

Magnetic fields will be generated in laser-produced plasmas whenever the density and pressure profiles become noncollinear.[13] Large dc magnetic fields have been observed[10] in laser-produced plasmas and have been associated with the finite-sized nature of the laser beam. Modest asymmetries (O(2:1)) on the interior of the laser beam also generate large magnetic fields[14]. Laser asymmetries generate pressure variations at the ablation surface which provides the source for the magnetic fields. As a result of the ablation process, these fields are shed from the ablation layer and convected into the blowoff, filling the overdense region. We show here that these fields can give rise to strong thermal flux inhibition. It should be noted that laser asymmetries (O(2:1) or larger) have been inherent in nearly all thermal flux inhibition experiments.

A simplified model equation governing the development of the magnetic field is

$$\frac{\partial \vec{B}}{\partial t} + \vec{u}\cdot\nabla\vec{B} = -\frac{c}{en_e^2}\nabla n_e \times \nabla p_e - \vec{B}\nabla\cdot\vec{u} \qquad (1)$$

where c is the speed of light and e, n_e and p_e are the electron charge, number density and pressure, respectively. The first term on the RHS is the baroclinic source term which generates magnetic fields (and vorticity) whenever the density and pressure gradients are noncollinear. Eq. 1 is an approximation to the complete magnetic field expression[7] as obtained from the generalized Ohm's Law which also contains the resistive diffusion, magnetic pressure and thermal-force terms. These terms have a very minor role in the simulations presented here. The resistive diffusion times for these fields are much longer than the width of the laser pulse and the magnetic Reynold's number is large ($R_m > 10$), both of which indicate that the fields are "frozen-in". The magnetic pressure is seldom more than a few percent of the plasma pressure. At the ablation layer, where the fields are being generated, the product of the electron cyclotron frequency (ω_{ce}) and the electron-ion collision time (τ_{ie}) is very small ($\omega_{ce}\tau_{ie} \lesssim 10^{-2}$). This implies that the thermal-force term[15] is not playing a role in this region. When $\omega_{ce}\tau_{ie} > 1$ in the blowoff region, the thermal force term is typically an order of magnitude smaller than the baroclinic source term. An examination of the complete expression for the thermal conductivity coefficients in a magnetized plasma[7] shows that the ratio of the coefficient for transport across a magnetic field to the coefficient for an unmagnetized plasma is < 0.10 for $\omega_{ce}\tau_{ie} = 1$ and $Z > 6$. This ratio is ~ 0.02 for $\omega_{ce}\tau_{ie} \approx 4$. $\omega_{ce}\tau_{ie}$'s of this order are easily attained in this parameter regime.

We model the interaction of moderate to high intensity (10^{13} W/cm$^2 \lesssim I \lesssim 10^{15}$ W/cm^2), short pulse ($\lesssim 1$ ns), 1.054 μm laser light on thick (25 μm, 5.5 mg/cm^2) planar carbon targets with our hydrodynamics model, FAST2D.[16] For the results presented here the nearly sinusoidal periodic variation in

incident intensity is 73% ($\Delta I/\langle I\rangle = 0.73$, $\Delta I = I_{max} - I_{min}$) with a spatial wavelength of 50 μm and a gaussian pulse length of 1 ns FWHM. FAST2D is a fully two-dimensional Cartesian code with a sliding Eulerian grid with variable grid spacing. The ablation layer is finely resolved with a grid spacing of 0.10 μm. Finer zoning produces no discernable difference in the results. The refined subzoning follows the ablation front throughout the course of the run. FAST2D solves the ideal hydrodynamic equations using the flux-corrected transport (FCT)[17] algorithms with a two-dimensional magnetized plasma thermal conduction routine which includes the thermal flux perpendicular to both the magnetic field and the temperature gradient (the Righi-Leduc term) and the complete charge dependent magnetized transport coefficient. The laser energy is absorbed classically with 10% of the irradiance that reaches critical being absorbed resonantly. The code has been extensively documented against experimental data[18] and is discussed in some detail in Ref. 16 and references therein.

Figure 1 shows the magnetic field structure at two different times for a typical 1 ns FWHM run (Case E of Table I). For this run the spatially averaged peak incident intensity is 2.6×10^{14} W/cm^2 (3.6×10^{14} W/cm^2 - 1.7×10^{14} W/cm^2) and the spatially averaged absorbed intensity is 1.2×10^{14} W/cm^2, yielding 45% absorption. The shedding of the fields from the target as a result of the ablation process is evident at 0.4 ns. By 0.6 ns this structure has nearly separated from the target and is being convected downstream. The magnetic field structure effectively fills the region between ablation and critical. An identical calculation except with the magnetized transport turned off gives 60% absorption and peak magnetic

fields of order 700 kG (Case D), down from 3MG in the previous case. The numerical results are summarized in Table I.

TABLE I

Data Comparison at Peak of Laser Pulse

	A U	B M	C U	D U	E M	F M
$\langle I \rangle_I$	1.6	1.6	9.0	25.0	25.0	65.0
$\langle I \rangle_A$	1.5	1.0	7.2	16.0	12.0	23.0
P	3.3	2.4	9.9	22.8	12.8	18.5
$\dot{m}$	1.0	0.7	2.3	3.5	1.5	1.74
v	1.4	0.94	1.7	5.0	2.8	3.7
$\Delta p/p$	4.0	24.0	6.0	3.0	17.0	34.0
D_{ac}	47.0	16.0	144.0	236.0	117.0	194.0
L	143.0	156.0	127.0	190.0	400.0	390.0
B	0.3	6.0	0.73	0.67	3.0	7.0

M(U) are cases with the magnetized (unmagnetized) transport.

$\langle I \rangle_I$ ($\langle I \rangle_A$) is the spatially averaged incident (absorbed) laser intensity ($10^{13} W/cm^2$); P(Mb) is ablation pressure; $\dot{m}$ (10^5 gm/cm^{2}s) is mass ablation rate; v(10^6cm/s) is target velocity; $\Delta p/p$ is variation in ablation pressure across target; D_{ac} (μm) is distance between ablation and critical; L(μm) is density scalelength at 1/4 critical; B(MG) is peak magnetic field strength.

The magnetic fields influence the evolution of the laser plasma interaction in several ways. The fields are generated at the ablation surface early in the pulse near where the gradient in the laser intensity is the largest; approximately midway between the intensity maximum and minimum. The fields are shed from the ablation layer and reduce the longitudinal transport. The Righi-Leduc term, which controls the flux perpendicular to both B and ∇T, plays a dual role here. This term produces a transverse heat flow from the cooler to hotter regions in the underdense plasma. This is the source for the thermal instability discussed in the literature.[19] Fortunately this instability is self-limiting. An increase in the transverse temperature gradient in the underdense magnetized plasma also increases the rate of heat flux out of the system back towards the laser. Also, an increase in temperature in the region where the laser is hottest reduces the amount of classical absorption there and effectively turns off the driving term for this instability. The temperature throughout the underdense region is increased as a result of the inhibited transport thus reducing the amount of classical absorption.

Figure 2 compares the density (ρ), pressure (p) and temperature (T) profiles which have been spatially averaged across the system for magnetized transport and unmagnetized transport for approximately the same absorbed intensity. Relative to the unmagnetized case, the profiles for the magnetized case show a reduced ablation pressure, steeper temperature gradient and higher temperature in the blowoff and flatter density profile.

The mass ablation rate is very sensitive to the thermal transport. Fig. 3 compares the mass-ablation rates between the inhibited and uninhibited cases as a function of average absorbed intensity. For the uninhibited transport case $\dot{m} \propto I^{0.53}$, which agrees well with experiment and theory in the low intensity regime[20] ($I < 2 - 3 \times 10^{13}$ W/cm^2) where the transport is not expected to be strongly inhibited. For the inhibited transport case the mass ablation rate is a strong function of the absorbed intensity and shows two fairly distinct scaling regimes: $\dot{m} \propto I^{.35}$ for $I < 10^{14}$ W/cm^2, and $\dot{m} \propto I^{.18}$ for $I > 10^{14}$ W/cm^2. Also shown in Fig. 3 are the mass-ablation rates from a 1-dimensional simulation (FAST1D)[21] with an imposed flux inhibition factor of 0.03. The agreement is quite good.

In summary, we have shown that the observed thermal flux inhibition can stem directly from the strong magnetic fields generated at the ablation layer as a result of modest laser asymmetries. With one notable exception[22], where little, if any, flux inhibition was observed, laser asymmetries have been inherent in nearly all flux inhibition experiments. The multimegagauss magnetic fields are shed from the ablation layer and fill the overdense region strongly influencing the thermal transport. The self-consistent treatment of thermal transport in this environment shows strong thermal flux inhibition which is manifested by the following observations: (1) reduced ablation pressures, (2) reduced implosion velocities, (3) reduced mass ablation rates, (4) density profile flattening and (5) reduced classical absorption; all of which have been experimentally observed. The spatially averaged mass ablation rates obtained from the

self-consistent two-dimensional model agree well with a one-dimensional model using an imposed flux inhibition factor of 0.03.

We gratefully acknowledge helpful discussions with J.P. Boris and S.E. Bodner. This work was supported by the U.S. Department of Energy and the Office of Naval Research.

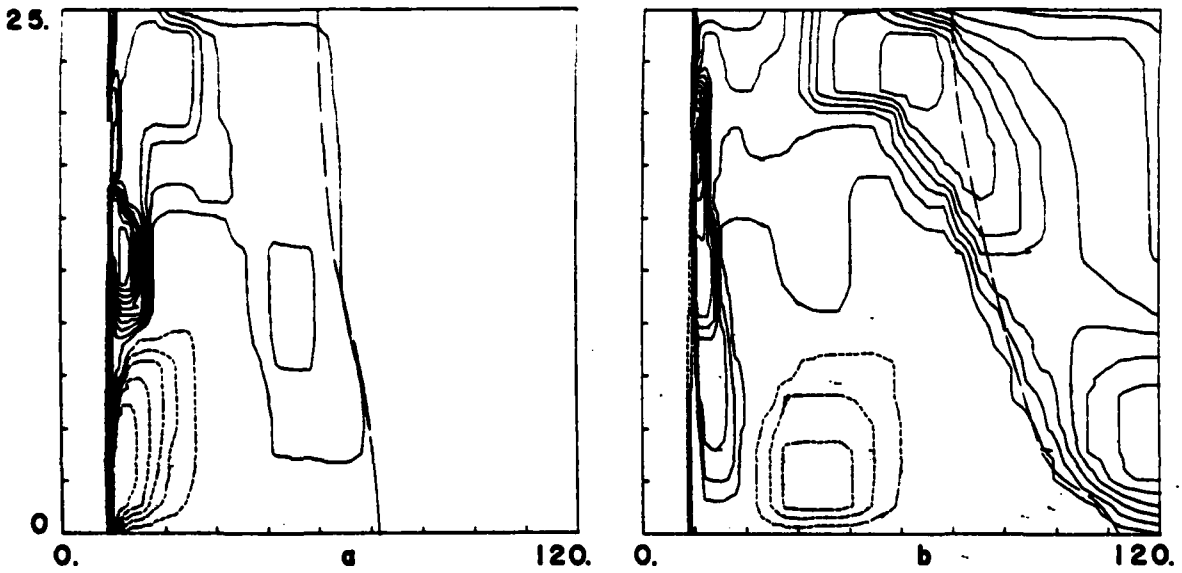

Figure 1

Contours of magnetic field strength in 10% increments of the maximum at 0.4 ns (a) and 0.6 ns (b) for Case E. Solid (dashed) contours indicate a field direction out of (into) the plane. The long dashed line is the critical surface. The dimensions are in microns. The laser is impinging the foil from the right. One half of a wavelength is shown with the laser intensity at its minimum at the bottom edge of each picture. The ablation surface is at 10 μm. The peak field strengths are 2.3 MG (a) and 2.8 MG (b).

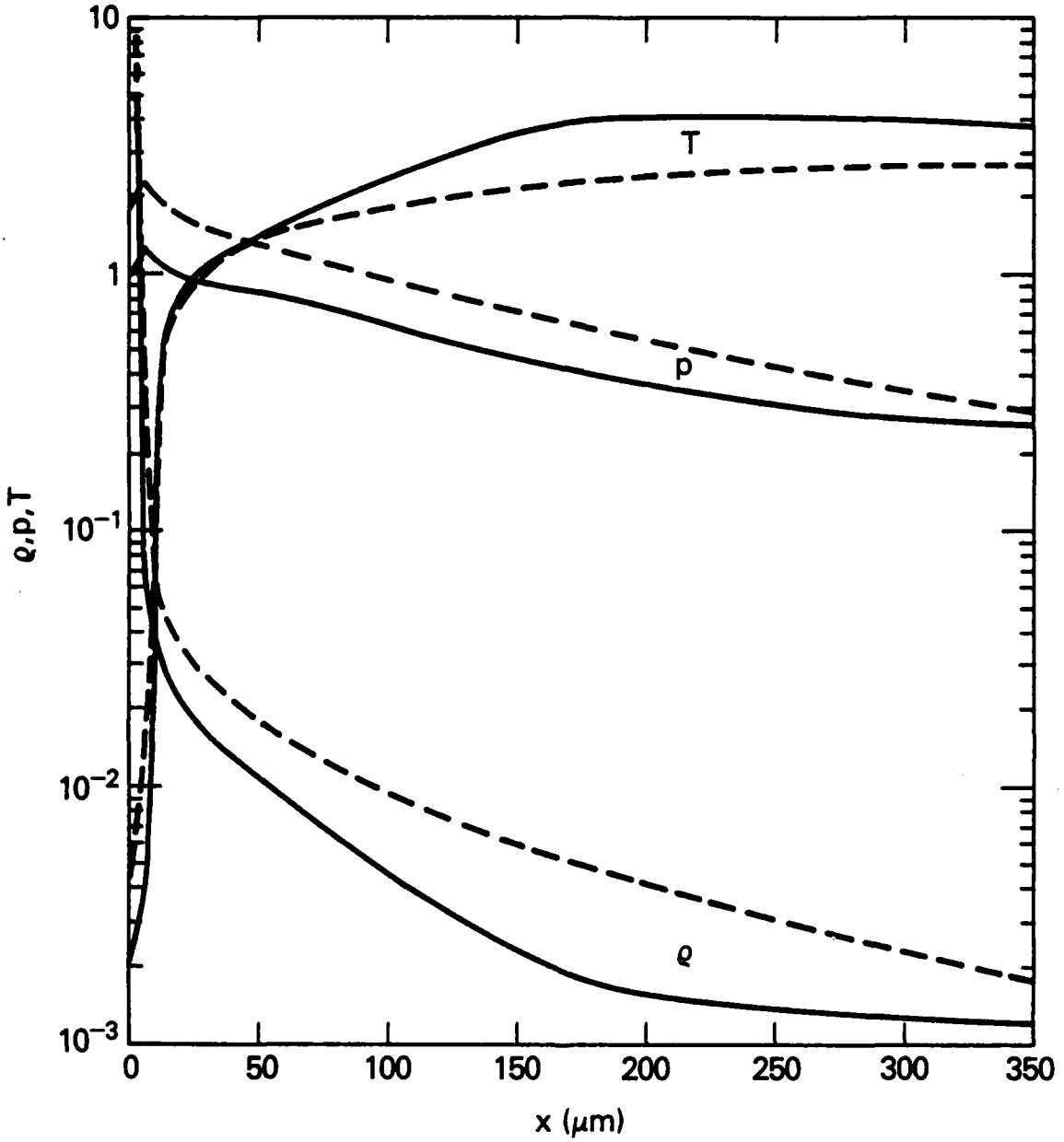

Figure 2

Comparison of the density (ρ, gm/cm^3) pressure (p, 10^{13} dynes/cm^2) and temperature (T, kev) profiles at the peak of the 1 ns pulse between the magnetized transport (——, Case E) and the unmagnetized transport (- - - -, Case D).

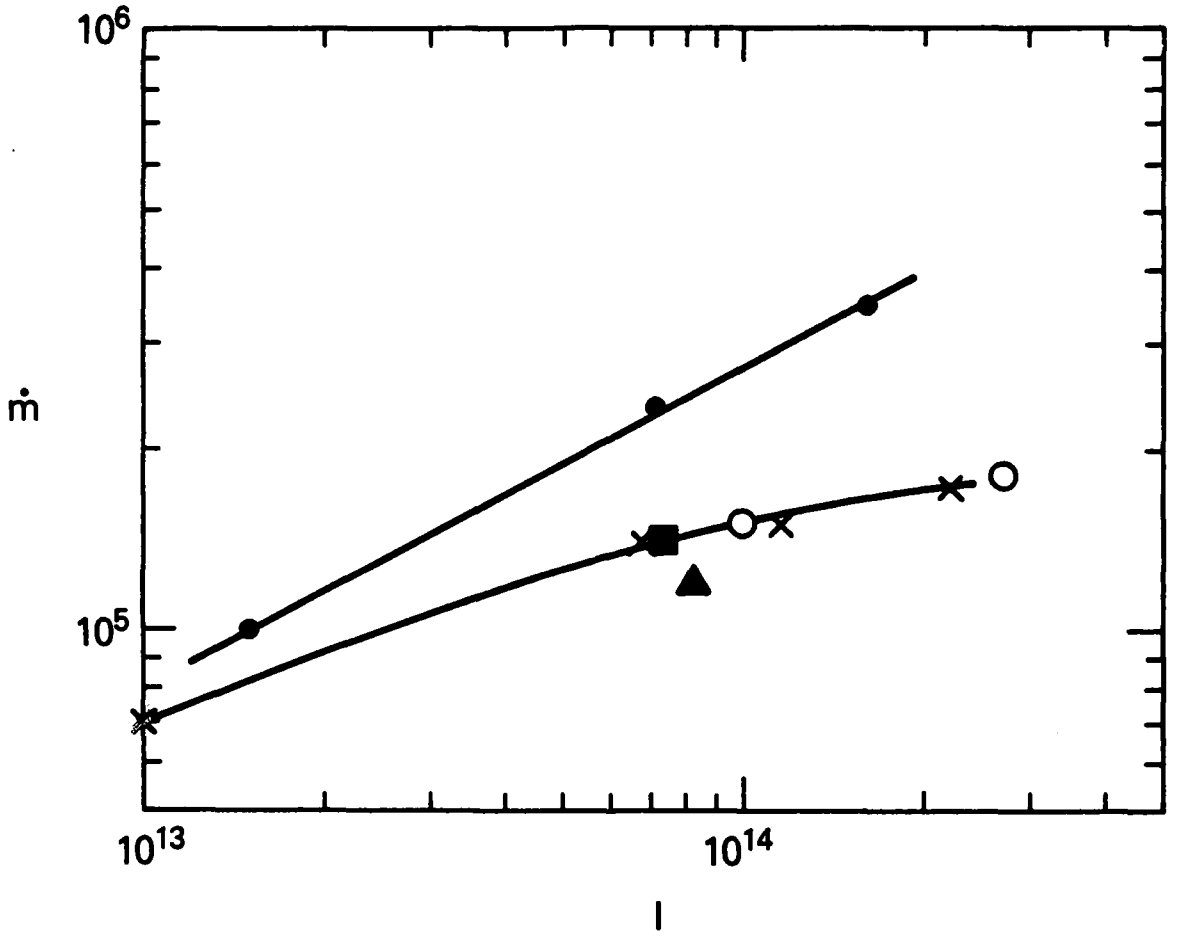

Figure 3

Mass ablation rate (gm-cm^2/s) as a function of the spatially averaged absorbed intensity (W/cm^2) for the unmagnetized (●) and magnetized (x) transport and the one-dimensional results with f = 0.03 (0). ▲ is the result for 1/2 ns FWHM pulse and ■ is the result for a 1/4 ns FWHM pulse.

REFERENCES

1. R.C. Malone, et al., Phys. Rev. Lett. 34, 721 (1975).
2. D.T. Attwood, IEEE J. Quant. Electron, QE-14, 909 (1978).
3. F.C. Young, et al., Appl. Phys. Lett. 30, 45 (197[illegible].
4. R. Benattar, et al., Phys. Rev. Lett. 42, 766 (1979).
5. J.S. Pearlman and J.P. Anthes, Appl. Phys. Lett. 27, 581 (1975).
6. W.C. Mead, et al., Lawrence Livermore Laboratory Report No. UCRL-89335, 1983 (to be published).
7. S.I. Braginskii, Rev. Plasma Physics 1, 205 (Consultants Bureau, New York, 1965).
8. W. M. Manheimer, Phys. Fluids 20, 265 (1977).
9. A. Ramani and G. Laval, Phys. Fluids 21, 980 (1978).
10. J.A. Stamper, et al., Phys. Rev. Lett. 26, 1012 (1971).
11. C.E. Max, et al., Phys. Fluids 21, 128 (1978).
12. D.R. Gray and D.J. Kilkenny, Plasma Phys. 22, 81 (1980); A.R. Bell, et al., Phys. Rev. Lett. 46, 243 (1981); J.P. Matte and J. Virmont, Phys. Rev. Lett. 49, 1936 (1982).
13. Yu. V. Afanas'ev et al., Zh. Eksp. Teor. Fiz. 74, 516 (1978). [Sov. Phys. JETP 47, 271 (1978)].
14. M.H. Emery, et al., IEEE Int. Conf. Plasma Science, 501 (May, 1983), NRL Memorandum Report 5089 (1983), "Vortex Shedding and Laser Ablation". (AD-A133 467)
15. D.G. Colombant and N.K. Winsor, Phys. Rev. Lett. 38, 697 (1977).
16. M.H. Emery, et al., Phys. Rev. Lett. 48, 253 (1982), Phys. Rev. Lett. 48, 677 (1982) and Phys. Fluids (to be published).
17. J.P. Boris and D.L. Book, Methods Comput. Phys. 16, 85 (1976).

18. P.J. Moffa et al., Naval Research Laboratory Report No. 4369, 1980 (unpublished); P. G. Phys. Fluids 26, 3650 (1983); R.R. Whitlock et al., Phys. Rev. Lett. 52, 819 (1984).

19. D.A. Tidman and R.A. Shanny, Phys. Fluids 17, 1207 (1974).

20. J. Grun, et al., Phys. Fluids 26, 588 (1983).

21. J.H. Gardner and S.E. Bodner, Phys. Rev. Lett. 47, 1137 (1981).

22. B. Yaakobi et al., LLE Report No. 136 (1982), and Proc. Transport Workshop, University of Rochester (1983).

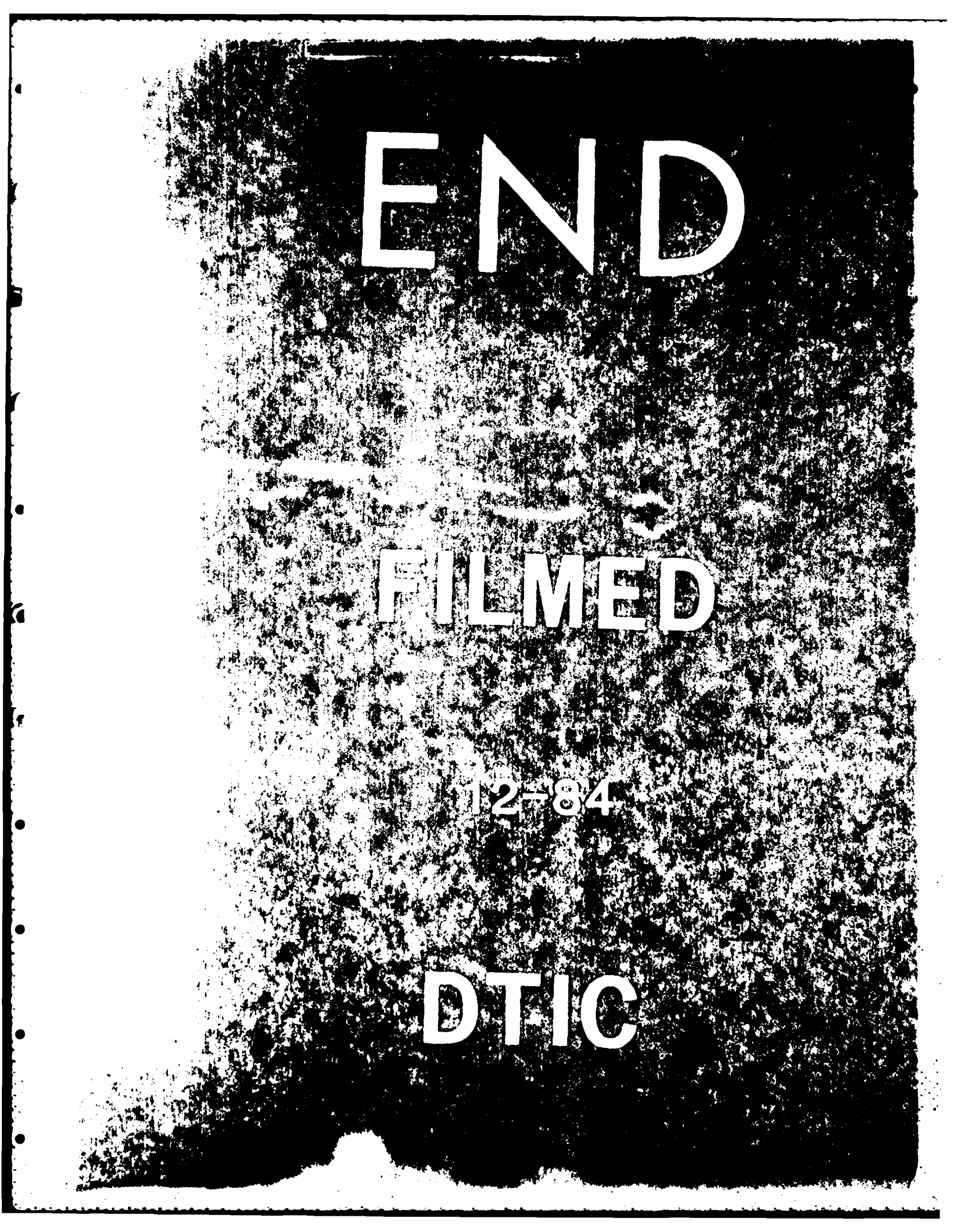
END
FILMED
12-84
DTIC